Chapter 4

A Discussion on the Detachment Structural Deformation and Its Influence on Pore Structure Evolution in Shale on the Western of the Xuefeng Mountain, South China

Mingliang Liang, Zongxiu Wang, Linyan Zhang, Huijun Li, Wanli Gao and Chunlin Li

Additional information is available at the end of the chapter

http://dx.doi.org/10.5772/intechopen.72245

Abstract

Detachment structures occur widely in the crust, and it is the commonest and most important deformation type developed in the region between orogenic belts and basins. Organic-rich shale, as the weak layers, usually acts as slippery layers in detachment structural deformation systems. The "comb-like" and "tough-like" fold belts on the western side of the Xuefeng Mountain result from the multilayer detachment, and their formation is different from the typical Jura type structures. The reason is that there are several detachment layers and detachment systems in the stratigraphic column from the Neoproterozoic upwards to the Mesozoic in the study area. As the stress decoupling role, the shale slippery layers tend to undergo strong deformation in the detachment systems and impacted on pore structure evolution in the shale. In order to obtain the detachment structural deformation and its influence on pore structure evolution in shale on the Middle and Upper Yangtze, the structural and textural, geochemical and mineralogical properties analysis, porosity and pore structure feature investigations are performed using shale samples collected from the same shale bed of the Longmaxi Formations (Lower Silurian) of Western of the Xuefeng Mountain, South China.

Keywords: Western of the Xuefeng Mountain, detachment deformation, tectonic deformed shale, Longmaxi shales, pore structure evolution

1. Introduction

Detachment structures occur widely in the crust, which is the result of the shearing occurring between a competent rock and an uncompetent rock, include many different types of

structures such as detachment folds and hybrid fault-propagation folds. Recently, a series of models of the detachment has been brought forwards, and the kinematics and mechanism of detachment folds is also an important branch in the studies of the thrust tectonics [1–6]. The typical detachment folds are those in the Jura Mountain in the Alps orogenic belt, in the foreland region of the Appalachian orogenic belt and in the foreland region of Cordillera orogenic belt [1, 7, 8]. And, many researches have also been carried out on the thrust tectonics in China since 1960 [9–19]. The main characteristic of these detachment folds is that they formed on the uncompetent layers such as the Triassic evaporates in the Jura Mountain [20–22]. However, most studies focus on the structure with single detachment layer, with few studies on the effects of the multilayer detachment on the derived structures except for those researches in the Jura Mountain and the Zagros Mountain [23, 24].

The deformation zone between the Huayin Mountain and Xuefeng Mountain in the eastern Sichuan, located in Middle and Upper Yangtze, is characterized by the multilayer detachments in the late Mesozoic, with discordant features in various structural styles (**Figure 1**). In the study region, the strata from the Cambrian up to the Jurassic are all covering layers in the basin, and the "comb-like" and "tough-like" fold belts result from the multilayer detachment. In terms of basic structural styles and mechanism, Liu argued that these thin-skinned structures resulted from differential erosion of box folds under the stress outside [25]. Ding et al. and Ding and Liu suggested that the folds in this region [26, 27], especially those comb-like folds, were the kink bands controlled by the buckling at the regional scale. Liu and Liu preferred that these folds were produced by the compression in the early Mesozoic and superimposed by the late

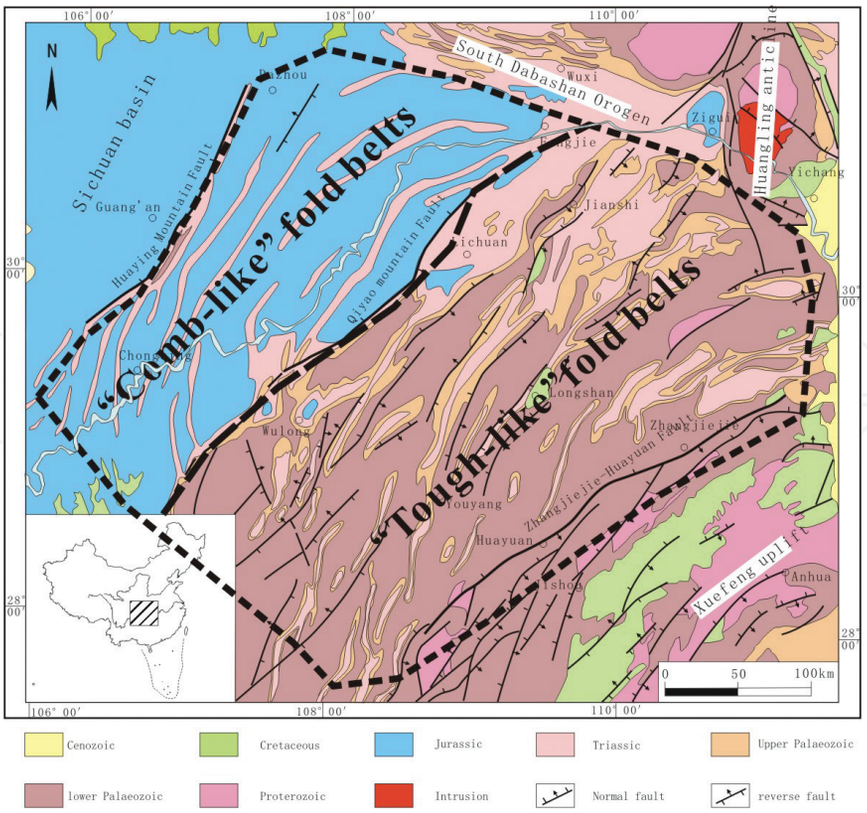

Figure 1. Geological map of western of the Xuefeng Mountain, South China.

extension [28]. Xu et al. divided this region into three structural layers [29], among which duplexes and fault-bend folds mainly form in the lower one, fault-bend folds and fault-propagation folds mainly form in the middle one and the detachment folds, fault-propagation folds and break-through structures mainly occur in the upper layer. Guo et al. further pointed out discordance occurring in various layers [30]. Yan et al. argued that multi-detachment thrusting due to the progressive compression from the southeast to the northwest resulted in the development of the structures in the study region. Two major detachment layers occur in these covering layers [10, 31], comprising the Lower Cambrian Niutitang Formation and Lower Silurian Longmaxi Formation (**Figure 2**). Organic-rich shale, as the weak layers, usually acts as slippery layers in detachment structural deformation systems in this study. The detachment layers in the study region show a wide range of deformation styles caused by shearing along the layers: A-type; S-C fabric; sheared puddings; cleavage and thrusts. The primary structure of deformed shale is damaged and the parallel bedding has almost disappeared due to deformation.

Previous studies have shown that the Upper and Middle Yangtze Plates have superior marine hydrocarbon geological conditions and immense potential for shale gas. Compared to North America, the geological conditions of gas shale reservoirs in South China are highly diversified and complicated due to the detachment structural deformation, which transformed the structure of shale seams and resulted in structure deformed shale with unique reservoir properties [32–35]. For example, as the first commercial shale gas field outside the North America, one of the most important controlling geological factors in the Fuling shale gas field in southeastern margin of the Sichuan Basin was strong structural deformation of shale [32, 33, 36]. It is necessary to study how pore structure develops in gas shale influenced by tectonic deformation. Ma et al. investigated the pore structure of the mylonitized shale sample by FESEM and N_2 adsorption analysis and found that the mylonitized shale has high specific surface area and high methane adsorption capacity [34]. Ibanez and Kronenberg have explained the deformational and microstructural changes under variable confinement

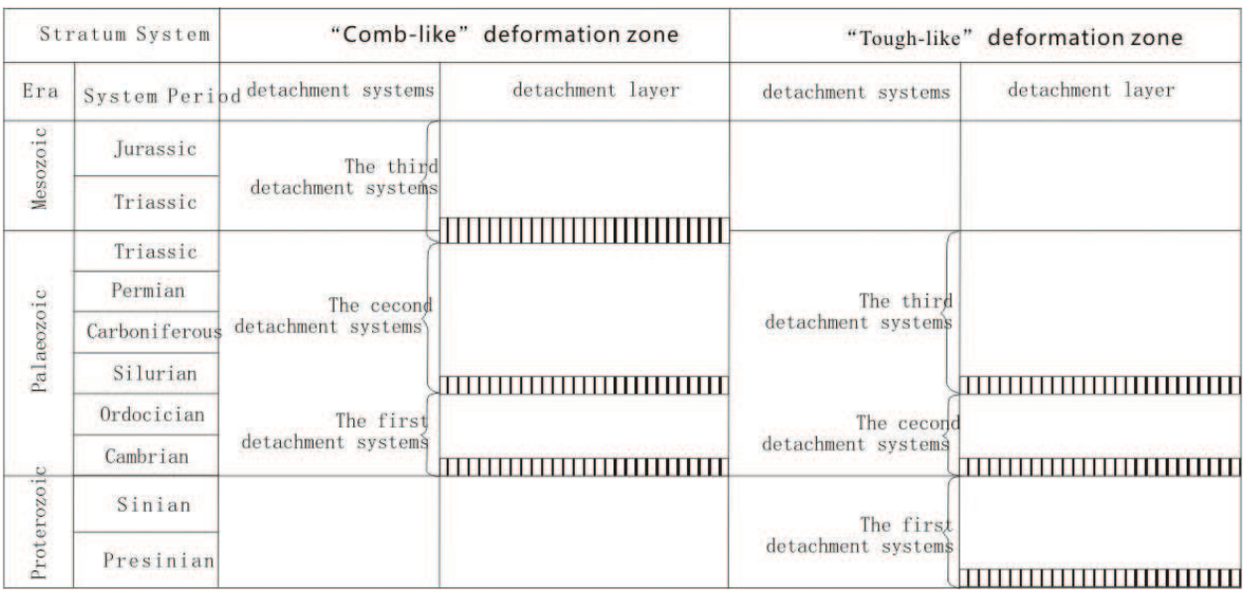

Figure 2. Distribution of detachment layers and constitution of detachment systems in western of the Xuefeng Mountain, South China.

for illite-rich shale [37]. Shale gas and coalbed methane (CBM) reservoirs are in formally grouped as unconventional because gas is trapped in part by sorption processes [38]. Several previous workers have focused on the pore characteristics and adsorption gas characteristics of tectonically deformed coals [39, 40], which provide references to the study on deformed shale. Although previous studies have provided useful insight to evolution of pore structure in shale during thermal maturity and in CBM related to deformation structures, the prediction of structural deformation change in pore structure of shale in geological condition still remains quite challenging. In the present study, pore structure feature investigations are performed using two sets of shale samples (deformed shale and undeformed shale) collected from the typical shale bed of the Longmaxi Formations (Lower Silurian) of Western of the Xuefeng Mountain, South China. The influence of structural deformation on pore structure was discussed.

2. Deformation of the detachment layers

There are two main detachment layers of shale in the covering layers in the study region, i.e., the Lower Cambrian Niutitang Formation and Lower Silurian Longmaxi Formation. These two detachment layers controlled the strong deformation of the study region during the late Mesozoic and showed different roles in different zones.

2.1. Deformation of the Cambrian system

The detachment layer is the Niutitang Formation ($Є_1n$) in the Lower Cambrian, which is mainly composed of black carbonaceous shale and black shale and about 70–200 m thick. This layer crops out in the region between Shizhu and Anhua-Xupu Fault, but the strong shearing along the layer only occurred in the region between the Cili-Dayong Fault and the Anhua-Xupu Fault.

Different types of small shear folds and thrust faults character the deformation of the detachment layer, including angular folds, congruous inverted folds, sheath folds and recumbent folds. B-type and A-type folds can be found (**Figures 3** and **4**). The fold hinges strike mainly northeast-southwest. However, the fold hinges of sheath folds trend northwest-southeast, which indicated the direction of shearing. The axial planes of these folds mainly dip to the southeast at the angle of 40–70°. Combined with sheath folds, top-to-the-northwest thrusting occurred along this detachment layer, which is similar to the deformation of the Xuefeng Mountain.

2.2. Deformation of the Silurian detachment layer

The Silurian detachment layer is composed of the Longmaxi Formation (S_1l) of the Lower Silurian. It is the thickest detachment layer (more than 2000 m) in the study region, which is mainly composed of shale with some silty mudstone and siltstone. This layer mainly distributes in Shizhu and Baojing; it also crops out to the west of Anhua-Xupu Fault. Field observations showed that the deformation of this layer mainly occurred in the region between Shizhu and Baojing (the region where the so-called narrow syncline style folds developed).

The B-type folding characters the deformation of the Silurian detachment layer. The congruent inverted fold is the main type of the folds in this layer (**Figure 5**). Most fold hinges strike

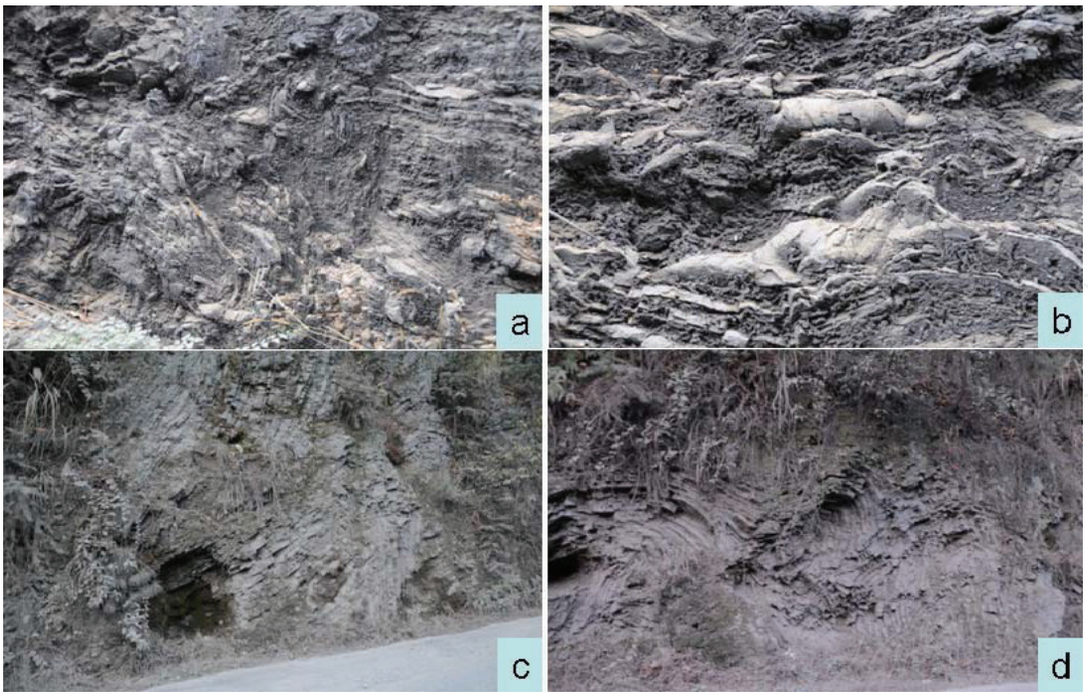

Figure 3. Shear folds formed by shear deformation in the lower Cambrian detachment layer. (a) A-type shear folding; (b) pencil structure indicates SE-NW shear (location: Labachong, Luoyixi Town, Yongshun County, Hunan); (c, d) B-type shear folding (location: Mengfu Village, Liangshuijing Town, Yuanling County, Hunan).

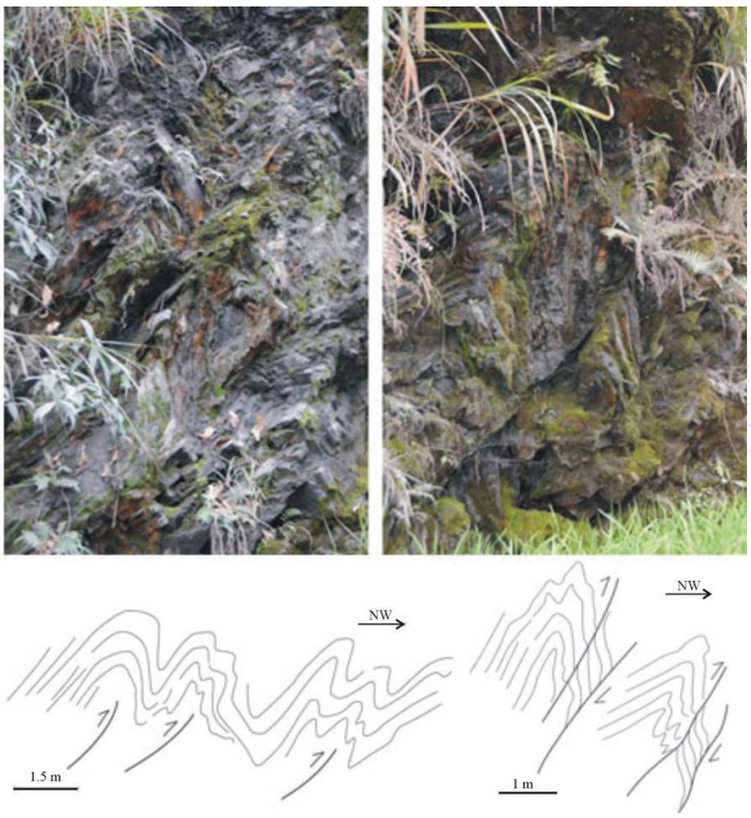

Figure 4. Assemblage of thrust faults and shear folds in the lower Cambrian (location: Fumeng Village, Liangshuijin Town, Yuanling County, Hunan).

Figure 5. B-type shear folds with SE dipping axial planes in the Silurian detachment layer (location: (a, b) Shaoha Village, Shaoha Town, Yongshun county, Hunan; (c, d) Heixi Town, Pengshui county, Chongqing).

northeast-southwest; some AB-type inverted folds whose hinges strike north-east are also found. The axial planes of these folds mainly dip to the southeast with dip angle ranging from 20 to 60°. And some inverted folds with axial plane dipping to the northwest are also developed. In addition, many minor thrust faults top to the northwest are also developed in the layer. These structures imply that the top-to-the-northwest thrusting parallel to the bedding is the main deformation mechanism, and the inverted folds with axial plane dipping to the northwest resulted from the back thrusting.

3. The discussion on mechanism of regional tectonic deformation

Many previous studies divided the deformation between the eastern Sichuan Basin and the Xuefeng Shan into the narrow anticline style fold belt, narrow syncline style fold belt and the basement-involved fold belt, which mainly resulted from the detachment folding and thrusting [10, 26, 27, 41–45]. This study showed that the so-called narrow-anticline style and narrow-syncline style folds in the eastern Sichuan Basin were named just after their geometries at regional scale; the exact original mechanism for these folds is different from that of the Jura type structures.

As mentioned in above sections, the deformation in the study region could be divided into two parts, one is the deformation of the detachment layers and the other is the deformation of rocks in the hanging walls. The bedding parallel detaching and many small-scale A-type,

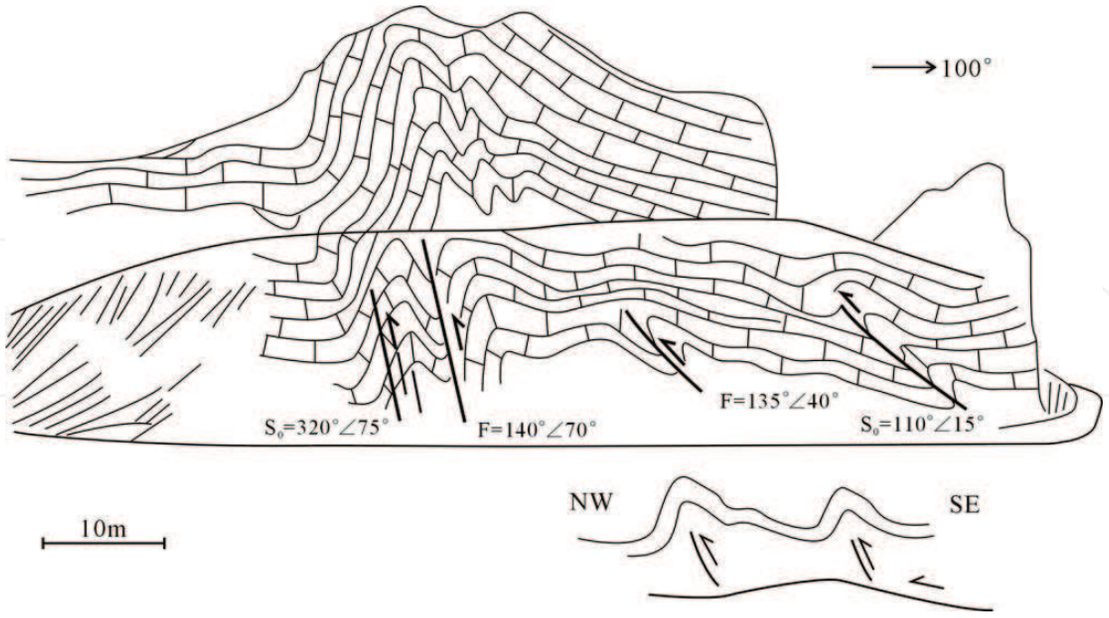

Figure 6. Widespread thrust folding in the eastern Sichuan Basin (location: Wanfo Village, Gaoleshan Town, Xianfeng County, Hubei).

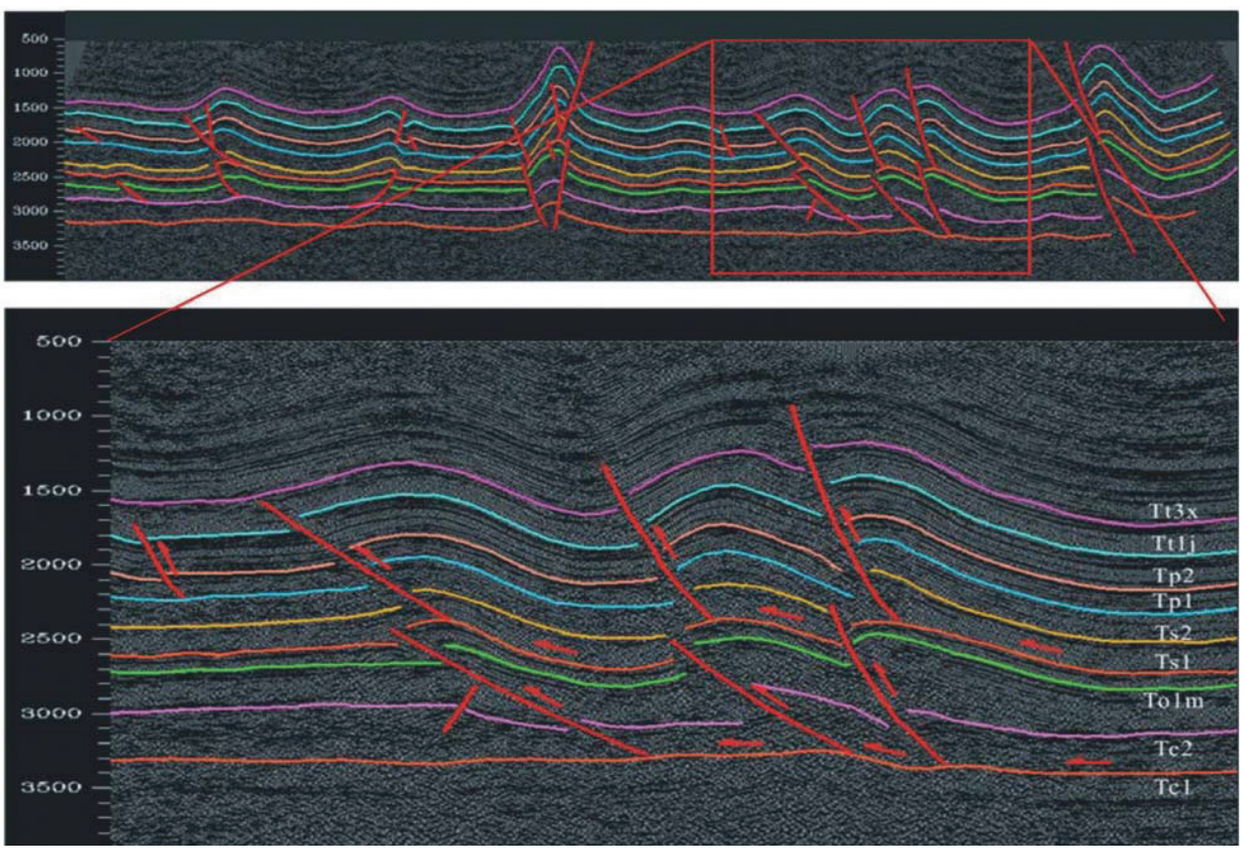

Figure 7. Multi-layer detaching-thrusting deformation section shown by the seismic reflection. Tt_3x, upper Triassic Xujiahe Fm; Tt_1j, lower Triassic Jialingjiang Fm; Tp_2, upper Permian; Tp_1, lower Permian; Ts_2, middle Silurian; Ts_1, lower Silurian; To_1m, lower Ordovician Meitan Fm; $T\epsilon_2$, middle Cambrian; $T\epsilon_1$, lower Cambrian.

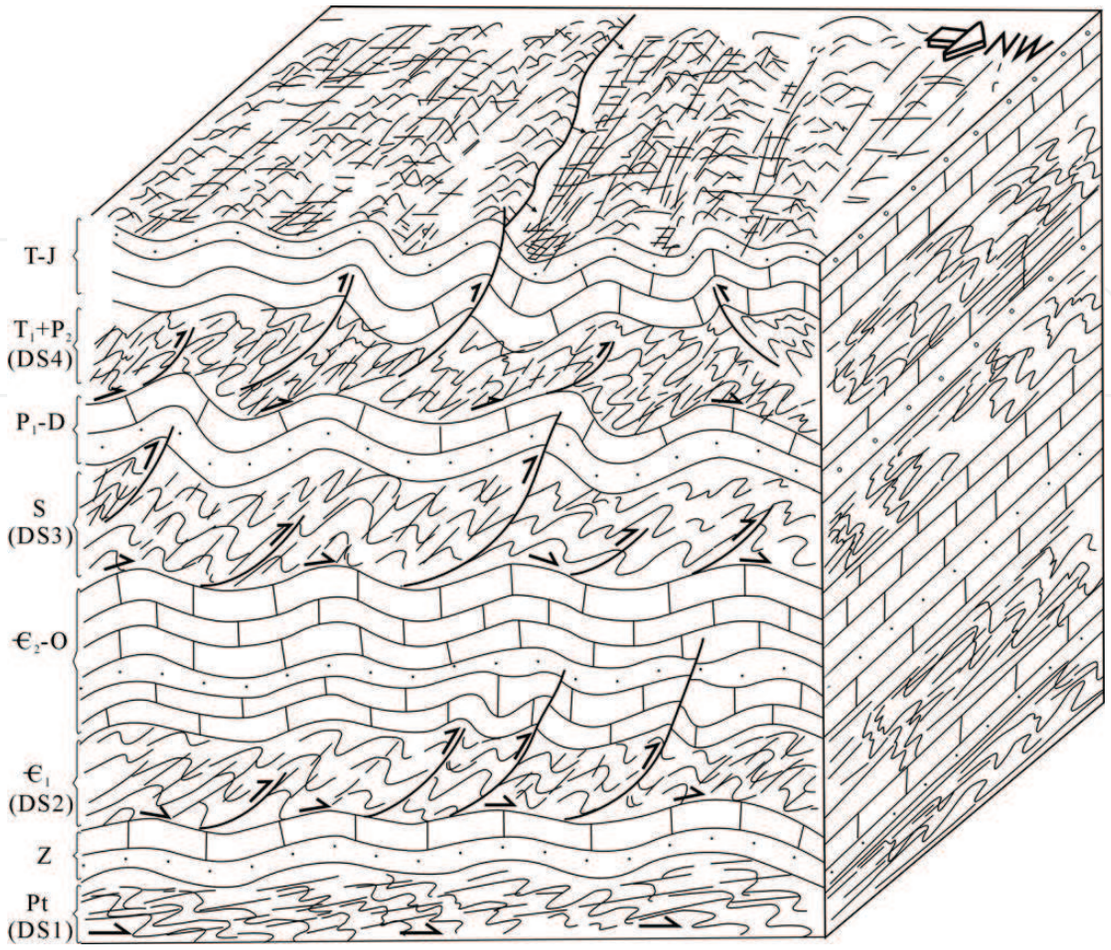

Figure 8. Block model of the deformation assemblage of multi-layer detachment and thrust fault between the Huayin Mountain and the Xuefeng Mountain. T-J, Triassic-Jurassic; T_1-P_2, lower Triassic-upper Permian; P_1-D, lower Permian-Devonian; S, Silurian; $Є_2$-O, middle Cambrian-Ordovician; $Є_1$, lower Cambrian; Z, Sinian; Pt, Precambrian (Banxi Gp); DS1, detachment layer and its number.

B-type and AB-type inverted folds, recumbent folds and small thrust faults character the deformation of the detachment layers, which generally imply the top-to-the-northwest detachment. And, the symmetrical large open folds and large reclined folds character the deformation of the non-detachment layers, and most geomorphic highs are located at the large reclined folds, such as the Huayin Shan, Tongluo Shan, Mingyue Shan, Fangdou Shan and Qiyao Shan.

Most anticlines between the Fangdou Shan and the Huayin Shan (where the narrow-anticline style folds developed) are narrow with steep northwest limbs dipping at 70–85° and shallow dipping southeast limbs dipping at 40–65°. Between the anticlines are the open synclines. And most northeast trending anticlines between the Fangdou Shan to the west and the Xuefeng Shan to the east (where the narrow-syncline style folds formed) are large open asymmetrical folds with steep northwest limbs and shallow southeast limbs except for some folds with steep southeast limbs such as the asymmetrical folds in Wanzhou along the east bank of the Yangtze River. The field observation showed that thrust faults often developed in the cores and steep limbs of these asymmetrical folds, and the thrust faults in the cores did not cut through the folds (**Figure 6**); similar characteristics could be found in the seismic profiles (**Figure 7**). These large reclined folds resulted from the thrusting; however, the thrust faults

derived from the bedding parallel shearing along the underlying detachment layers led to the deformation of overlying rocks. The above deformation was the results of thrusting and detachment, called as detachment-thrusting mechanism.

The deformation between the Huayin Shan and the Xuefeng Shan is the typical of multi-layer detachment. From the Cambrian System to the Jurassic System, the different deformations between four detachment layers and strata between detachment layers are discordant (**Figure 8**). The detachment and thrusting in every detachment layer controlled the deformation of the overlying strata. The main detachment layers controlling the deformation are different in different belts from the east to the west in the study region. Previous studies suggested that the so-called narrow-anticline style fold belt between the Huayin Shan and the Xuefeng Shan was controlled by the Silurian detachment, and the narrow-syncline style fold belt was controlled by the detachment layer between marine covering layers and the metamorphic basement, and these two types of folds are all typical Jura type detachment folds [10, 46].

4. Detachment layers in shale of Longmaxi Formation and its structural deformation characteristics

To obtain information about the influence of tectonic deformation on shale pore characteristics, the geochemical, mineralogical, structural and textural properties analysis, porosity and pore structure feature investigations are performed using two sets of shale (deformed shale and undeformed shale) collected from the same shale bed of the Longmaxi Formation (Lower Silurian) of southeast of Sichuan Basin, China. Previous studies have shown that the Upper and Middle Yangtze plates have superior marine hydrocarbon geological conditions and immense potential for shale gas. Compared to North America, the geological conditions of gas shale reservoirs in South China are highly diversified and complicated due to the detachment structural deformation, which transformed the structure of shale seams and resulted in structure deformed shale with unique reservoir properties. The detachment layers in the study region show a wide range of deformation styles caused by shearing along the layers: A-type; S-C fabric; sheared puddings; cleavage and thrusts. As the main detachment structure belt [35], the Longmaxi Formations shale layer developed multilayer subdivided slip structural deformation. The primary structure of deformed shale is damaged and the parallel bedding has almost disappeared due to deformation. The plastic deformation of shale is obvious, and the cleavage structure and cleavage surface are smooth with fine-grained powder coatings. The detachment fault mirrors (FMs), scratches and micro-fold deformation phenomena were commonly present in Longmaxi shale outcrops. A suite of samples were subset to two sets of deformed shale and undeformed shale for this study due to their variability of texture, fabric and structure properties (**Figures 9** and **10**). To evaluate the influence of detachment deformation on shale reservoir characteristics by comparing the deformed shale and undeformed sample subsets, 14 shale samples (9 undeformed samples from 3 beds) were collected from this Yongshun outcrop (**Figure 9**). However, not all the 14 samples were examined. All samples were analyzed to determine the organic geochemistry and mineralogy, the undeformed samples taken from same bed have similar composition

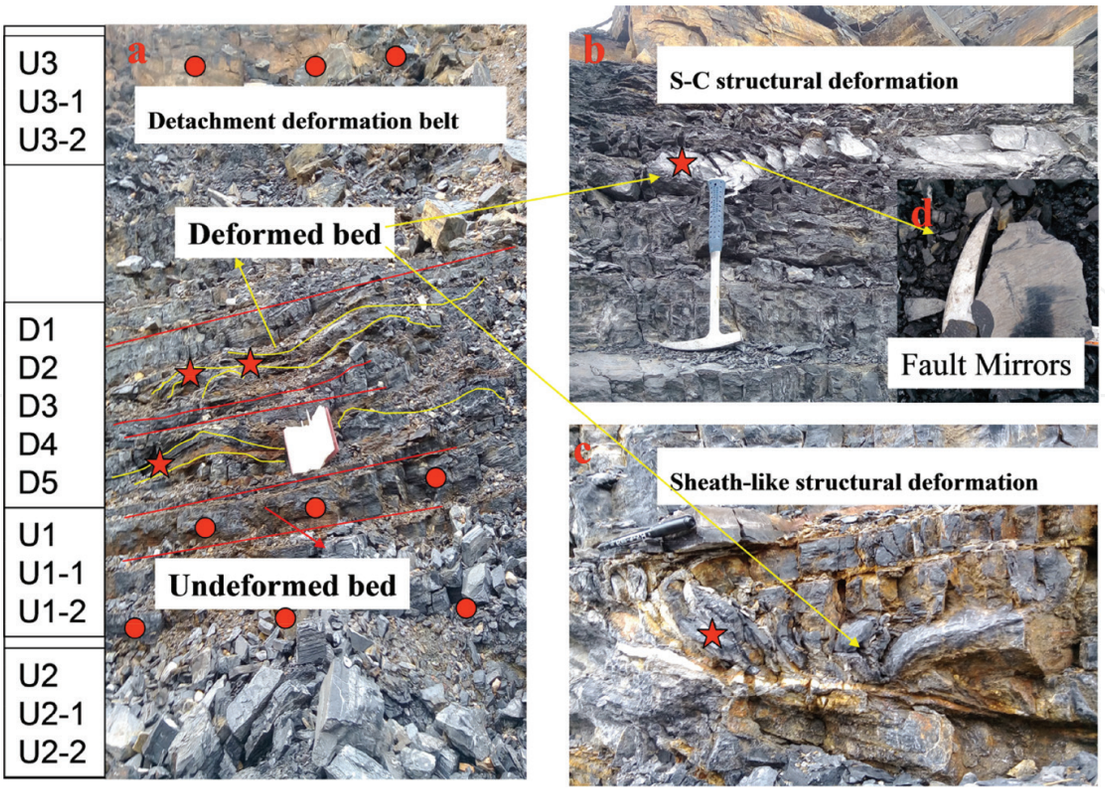

Figure 9. Location of study area is in southeastern Sichuan Basin, Yongshun, China. And the detachment structural deformation control across the Longmaxi Formations shale in this area. (a) The stratigraphic relationships and structural deformation characteristics of the samples, (b) S-C structural deformation shale, (c) Sheath-like structure deformation shale (d) Fault mirrors (FMs) of the deformed shale. ★ : Deformed shale samples, ● : Undeformed shale samples. The height of the notebook is 20 cm (a), length of the hammer is 38 cm (b) and the length of the pen is 14 cm (c). See **Figure 2** and **Table 1** for texture and structure properties of these deformed samples.

characteristics and eight samples (three undeformed samples and five deformed samples) were selected for mercury injection capillary pressure (MICP) and low-pressure gas (LPG) adsorption to determine the pore structure, including the porosity, pore-size distribution (PSD), surface area (SA) and pore volume (PV).

The sample number was abbreviated as U1, U2, U3 (Undeformed shale) and D1, D2, D3, D4, D5 (Deformed shale), the deformed samples subsets to strong deformed shale (D1, D2, D3) and weak deformed shale (D4, D5). The samples of U3 were collected from the thick sandy shale, and the other samples were collected from the thin siliceous shale. The stratigraphic relationships of the samples are shown in **Figure 9**. The features of the experimental samples are shown in **Table 1**. Before geochemical and mineralogical analyses, samples crushed to 180–200 mesh. The TOC content was collected using a Leco C/S-344 Carbon/Sulfur analyzer. The stable carbon isotope was determined using a Finnigan MAT 252 mass spectrometer. A 3Y–Leica DMR XP microscopy equipped with a microphotometer was used to measure the vitrinite reflectance values (VRo) of samples. Each sample was determined at least by 30 measurements on vitrinite particles. The crushed samples were mixed with ethanol, hand ground in a mortar and pestle and then smear mounted on glass slides for X-ray diffraction (XRD) analysis using a D/Max-III analyzer at 40 kV and 30 mA. The relative mineral contents were estimated and semi-quantified using the area under the curve for the major peaks.

http://dx.doi.org/10.5772/intechopen.72245

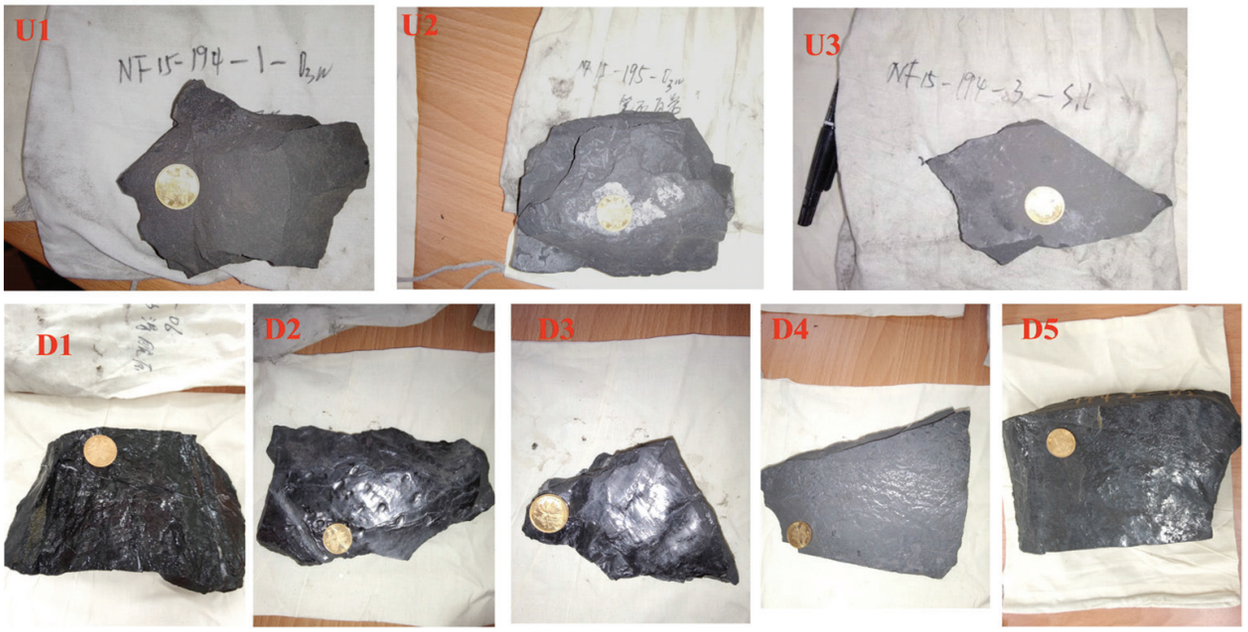

Figure 10. Undeformed shale and deformed shale samples; the sample ID was abbreviated as U1, U2, U3 (Undeformed shale) and D1, D2, D3, D4, D5 (Deformed shale). The undeformed shales have original parallel bedding, and the primary structure of shale can be observed. The detachment fault mirrors (FMs) can be observed on the deformed shales. And the deformed samples were subset to two sets of strong deformed shale and weak deformed shale due to their difference on the degree of deformation strength. The D1, D2 and D3 were strong deformed shales that the primary structure was damaged and the parallel bedding has almost disappeared due to deformation, and the fractures and mineral filling development in the strong deformed shales. The D4 and D5 were weak deformed shales that have original parallel bedding, and FMs developed in the surface of fault. The coin diameter is 20.5 mm.

Sample ID	TOC (%)	VRo (%)	δC_{13} ‰ (PDB)	Quartz (%)	Carbonate (%)	Clay (%)	Texture and fabric features of macroscopic hand specimens
U1	3.9	2.57	−30.4	41	nd	44	Undeformed shales. Shale primary structure can be observed. Shale has original parallel bedding
U2	2.5	2.78	−30.8	40	2	41	
U3	2.0	2.77	−30.9	34	11	33	
U-mean (9)	2.8	2.76	−30.7(3)	42	4.6	38	
D1	2.1	3.01	−30.6	77	nd	14	Strong deformed shales. The primary structure of shale is damaged and the parallel bedding has almost disappeared due to deformation. Fractures and mineral filling development. The plastic deformation of shale is obvious. Shale shows cleavage structure and cleavage surface is smooth with fine-grained powder coatings
D2	6.6	2.86	−31.0	64	nd	26	
D3	1.0	2.91	−31.3	77	nd	16	
D4	1.8	2.90	−30.6	46	nd	41	Weak deformed shales. Shale has original parallel bedding. Shale shows cleavage structure and cleavage surface is smooth with fine-grained powder coatings
D5	3.0	3.00	−31.1	71	nd	20	
D-mean (5)	2.9	2.93	−30.9	67	nd	23	

TOC, total organic carbon (%); VRo, vitrinite reflectance values (%); (Number), number of measured samples.

Table 1. The features of the experimental samples.

Sample ID	Gas absorption		MICP			Relative content* (%)		
	Micropore (μL/g)	Mesopore (μL/g)	Mesopore (μL/g)	Macropore (μL/g)	Porosity (%)	Micropore (%)	Mesopore (%)	Macropore (%)
U1	6.4	4.8	186.7	231.9	2.0	37.6	27.9	34.6
U2	5.7	8.4	175.5	122.9	1.6	28.5	42.0	29.4
U3	10.4	20.9	2198.4	330.0	7.5	30.3	60.6	9.1
D1	4.5	2.2	73.9	185.7	1.3	36.6	18.1	45.4
D2	5.3	6.7	73.8	143.3	1.6	21.2	26.8	52.0
D3	2.2	0.4	14.2	273.2	3.8	22.6	3.8	73.5
D4	4.5	3.8	148.7	172.1	2.5	28.5	23.8	47.7
D5	5.2	4.4	214.3	387.4	4.5	15.1	12.9	71.9

*The relative contents of different pore size distributions with PV were calculated by set the mesopore PV as referenced value.

Table 2. Pore volume characteristics of the samples.

To fully evaluate the pore size distribution and porosity, samples were crushed (2–5 mm), dried at 110°C and then preformed both mercury porosimetry and low pressure gas adsorption analyses. The mercury injection capillary pressure (MICP) analysis using a Poremaster GT60 and intruded with mercury from 1.5 to 60,000 Psi, the measured pressure range equates to the pore diameter range of 0.003–1000 μm (7–120,000 nm in this study). The pore size distributions of mesopores and macropores were determined using the Washburn equation [47]. The minimal pore diameter limit of 7 nm is within the mesopore range, and mercury porosimetry cannot detect micropores within the pore structure. Porosity is determined by mercury immersion (bulk density) coupled with helium pycnometry (skeletal density). Low pressure gas adsorption analyses have been used to measure the PSD both micropores and mesopores using both nitrogen adsorption at −196°C and carbon dioxide adsorption at 0°C by a Micromeritics ASAP 2020 HD88 analyzer. The PSD, PV and SA analysis of combined the N_2 and CO_2 gas adsorption by the same calculation models of density function theory (DFT) [48, 49]. The development of DFT models has led to a better understanding of adsorption processes in well-ordered systems compared to the more conventional models, used in the present study to analyzed N_2 and CO_2 gas adsorption data. The pore characteristics including SA, PV and PSD will be different between the two techniques (MICP and gas adsorption analyses) because of sample preparation, analytical models and calculation models; analysis method of combined the mercury intrusion and gas adsorption only used to determine the relative content percentage of micro-, meso- and macropores in this article by set the mesopores as a referenced values (**Table 2**).

5. Evolution of pore structure in the shale of detachment layers

It is believed that the shale composition controlled the pore structure character, and the diagenetic processes controlled the shale composition [38, 48, 50]. In the previous analysis, we

discussed the pore characteristic data obtained by different analytical methods of MICP and LPG separately [51]. **Figure 11** shows the correlation between porosity and pore volume for different pore diameters, indicating the positive relationship between porosity and micro- and mesopores PV ($R^2 > 0.85$) for undeformed shale, while the porosity of deformed shale was only related to the macropores PV ($R^2 = 0.77$). Such difference between the deformed and undeformed samples indicated that the micropores and mesopores (nanoscale pores) dominate the total porosity and controlled the diagenetic processes and shale compositions in the primary shale reservoir, while the macropores controlled the total porosity in the intense tectonic deformation shale. It is found that there were no significant changes in porosity between deformed and undeformed shale samples. In order to further study the evolution of pore size distribution in deformed shales, analysis method of combined the mercury intrusion and gas adsorption was used to determine the relative content percentage of micro-, meso- and macropores in this article by set the mesopores as a referenced value (**Table 2** and **Figure 12**). The balance of micro-, meso- and macropores were weakened in deformed shale samples, and the percentages of PV in different pore diameters were changed as macropores increased and mesopores decreased.

Organic matter can affect the evolution of pore structure, especially for different organic matter types and organic matter maturity. Jiang et al. reported the pore structure of a lacustrine oil shale in the Ordos Basin and indicated that the mesopores are dominant in samples [52]. Chen and Xiao measured the evolution of pore structure of artificially matured samples during an anhydrous pyrolysis, finding that the microporosity and mesoporosity increase with thermal maturity after the oil window stage [53]. The effect of organic matter on shale pore structure is mainly concentrated on micropore and mesopore [53–55] and achieved by the difference type and maturity. In the present study, all samples have a similar kerogen type and maturity stage, consistent with the similar micropores. Clay minerals can influence pore structure evolution and always have comparable organic contents. As compared to the deformed shale samples, the undeformed shale samples have higher values in micro-, meso-, total pore SA and adsorption quantity, because they have a higher clay content

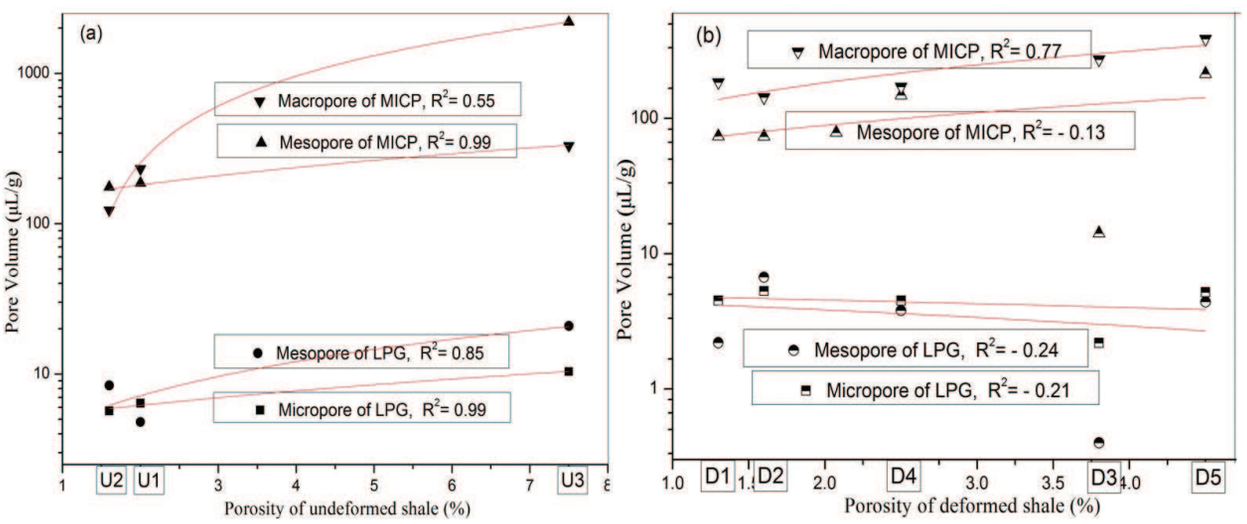

Figure 11. Relationship between total porosity and pore volume of micro-, meso- and macropores in shale samples from different analytic methods of LPG and MICP.

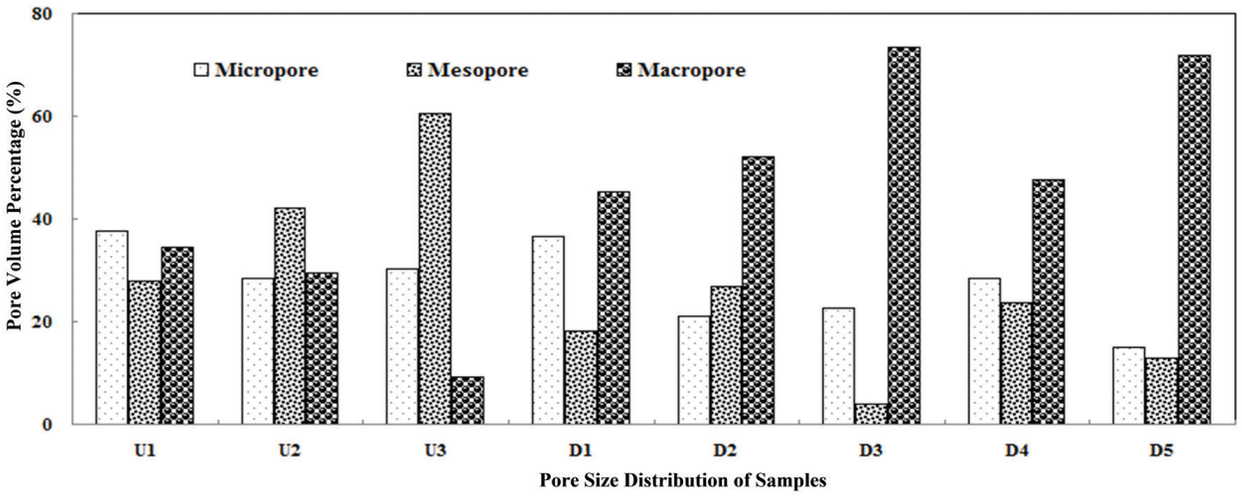

Figure 12. The pore volume percentages for shale samples.

rather than because of their undeformation. Ross and Bustin suggested that shales enriched in both clays and organics have the largest micropore volumes, suggesting a micropore contribution from both the organic and clay fractions. In the present study, the shale sample of D3, which is poor in clay and TOC, has the least micro- and mesopores. Kareem et al. found that the clay minerals are over-represented at the pore surfaces and in pore spaces compared to the other major minerals such as quartz and feldspar [56]. The knowledge of effective mineralogy complicated the influence of clay minerals on the pore structure. The biogenic quartz produced by precipitation during diagenesis with silica is derived from graptolite and radiolarians [57], which may also control the pore volume and structure in shales. This type of quartz affects microporosity significantly and has certain correlation to TOC content. There are no clearly defined relationships between quartz mineralogy and pore structure, because the micropore characteristics of the samples did not change with the quartz content in this study. Furthermore, the parts of extra quartz content in fracture filling of deformed shale may come from the hydrothermal source, after the tectonic deformation and fracture generations. The relationship between shale compositions and pore structure is not well reflected in the change of shale pore structure in deformed shale samples for the present study. There is no significant difference in organic matter content in deformed and undeformed samples, which agrees with a similar microporosity on all of the samples. All-scale pore structure analysis reveals that the deformed shale had notable higher macropores percentages than undeformed shale. At the same time, the total porosity and micropores were constant, suggesting that the evolution of pore structure in structural deformed shale was due to part of mesopores was disappeared due to compression of the tectonic stress, and macropores were generated due to the development of microcracks.

6. Conclusions

A series of comb-like folds and trough-like folds in eastern Sichuan Basin were the deformation controlled by multilayer detachment, which is different from the typical Jura type

detachment folds. Although the deformations between the Jura Mountain and eastern Sichuan look similar at the regional scale, their deformation mechanisms are different. There are many detachment layers occurring in the strata from the Neoproterozoic to the Mesozoic in the study region that controlled the deformation. Due to the multi-tectonic movement, shale reservoirs in China are highly diversified and complicated, which transformed the texture of shale beds and resulted in structure deformed shale with unique pore properties. The structural deformation has a significant effect on the evolution of pore size distribution, especially for the increase in the proportion of macroporous.

Acknowledgements

This research was funded by the Science and Technology Research and Development Program of China Petroleum and Chemical Corporation (No. P06088), Nonprofit Special Research Program (No. 200811015), Land Resource Survey Project of the Ministry of Land and Natural Resources, China (No. 1212010782003), Major State Research Development Program of China (No. 2016YFC0600202) and the China Geological Survey (CGS, No. DD20160183).

Author details

Mingliang Liang, Zongxiu Wang*, Linyan Zhang, Huijun Li, Wanli Gao and Chunlin Li

*Address all correspondence to: wangzongxiu@sohu.com

Institute of Geomechanics, Key Lab of Shale Oil and Gas Geological Survey, Chinese Academy of Geological Sciences, Beijing, China

References

[1] Suppe J. Geometry and kinematics of fault-bend folding. American Journal of Science. 1983;**283**:684-721

[2] Jamison WR. Geometric analysis of fold development in overthrust terranes. Journal of Structural Geology. 1987;**9**:207-219

[3] Poblet J, McClay K, Storti F, Munoz JA. Geometries of syntectonic sediments associated with single-layer detachment folds. Journal of Structural Geology. 1997;**19**:369-381

[4] Marrett R, Bentham PA. Geometric analysis of hybrid fault-propagation/detachment folds. Journal of Structural Geology. 1997;**19**(3-4):243-248

[5] Liu C, Zhang YK, Shi B. Geometric and kinematic modeling of detachment folds with growth strata based on Bézier curves. Journal of Structural Geology. 2009;**31**:260-269

[6] McClay KR. Glossary of thrust tectonics terms. In: McClay KR, editor. Thrust Tectonics. Chapman and Hall; 1992. pp. 419-433

[7] Rich JL. Mechanics of low-angle overthrust faulting illustrated by Cumberland thrust block, Virginia, Kentucky and Tennessee. Bulletin of the American Association of Petroleum Geologists. 1934;**18**:1584-1596

[8] Collet LW. The Structure of the Alps. Glasgow University Press; 1964

[9] Zhu ZC. On Jura-type fold (S. China) and its mechanism. Earth Science-Journal of China University of Geosciences. 1983;**3**:45-53

[10] Yan DP, Zhou MF, Song HL, Weng WX, John M. Origin and tectonic significance of a Mesozoic multi-layer over-thrust system within the Yangtze block (South China). Tectonophysics. 2003;**361**(3-4):239-254

[11] Chen HJ, Yin YN. Calling for opening up oil/gas exploration frontiers in overthrust belt-a discussion on the distribution of oil controlled by the southern Jiangsu Overthrust Belt. Petroleum Geology and Experiment. 1983;**2**:5-15

[12] Zhu ZC, Ye JL, Yang KG. On thrust-nappe and gliding-detachment on both sides of Mufushan-Jiuling uplift and asymmetrical tectonic architecture of mountain. Earth Science-Journal of China University of Geosciences. 1987;**5**:55-62

[13] Li BL, Sun Y, Zhu WB, Guo JC, Wen SH. Study on the layer slip parameter systems in the eastern Sichuan. Journal of Southwest Petroleum Institute. 2001;**23**:29-33

[14] Sun Y, Jia CZ, Jiang YJ. Determination of physical parameters of rocks and establishment of regional layer-slip systems in the northern Tarim area. Chinese Journal of Geophysics. 1996;**39**(5):660-671

[15] Gao XS, Liu SG, Guo GA. Structural styles and relationships to hydrocarbon accumulation in the northeast of Central Sichuan. Journal of Mineralogy and Petrology. 1998;**18**:167-170

[16] Feng CM, Liu J, Song LJ. Formation mechanism of the tectonic deformation belt and the prognosis of favorable oil and gas exploration areas in the middle and upper Yangtze Valley. Acta Geoscientica Sinica. 2008;**29**(2):199-204

[17] Tang LJ, Yu YX, Yang WJ, Peng GX, Lei GL, Jin WZ, Wan GM. Internal deformation features of detachment layers in the front of the Kuqa foreland fold-thrust belt. Geology in China. 2006;**33**:944-951

[18] Tang LJ, Guo TL, Jin WZ, Yu YX, Li RF. Main structural styles and deformation mechanisms in the Northern Sichuan Basin, Southern China. Acta Geologica Sinica (English edition). 2008;**82**:543-553

[19] Wang GL, Wang X, Wang WJ. Study on Detachment Structures. Beijing: Science Press; 1992

[20] Buxtorf A. Prognosen und befunde beim Hauesnsteinbasis und Grenchenberg-tunnel und die geologie des Juragebirges. Ver-handlungen der Naturforschenden Gesellchaft in Basel. 1916;**27**:184-205

[21] De Sitter LU. Structural Geology. New York: McGraw-Hill; 1956

[22] Laubscher HP. Fold development in the Jura. Tectonophysics. 1977;**37**:337-362

[23] Donatella M, Hemin AK, Massimiliano RB. Structural evolution of a fold and thrust belt generated by multiple decollements: Analogue models and natural examples from the northern Apennines (Italy). Journal of Structural Geology. 2006;**28**:185-199

[24] Hemin AK, Bruno CV. The effect of decollement dipongeometry and kinematics of model accretionary wedges. Journal of Structural Geology. 2003;**25**:1445-1450

[25] Liu SZ. My opinion of structural pattern of thin-skinned structure in East Sichuan. Acta Geologica Sichuan. 1995;**15**:264-267

[26] Ding DG, Guo TL, Zhai CB. Kink structure in the West Hubei and East Chongqing. Petroleum Geology and Expeximent. 2005;**27**:205-210

[27] Ding DG, Liu GX. Progressive deformation in Yangtze plate-series 2 of the southern structure studies. Petroleum Geology and Expeximent. 2007;**29**:238-246

[28] Liu XF, Liu CX. Analysis of structural styles at the juncture of Chongqing, Hubei and Hunan. Journal of Jianghan Petroleum Institute. 2002;**24**:1-4

[29] ZY X, Li DC, WZ L, Lin K, Liu CY. Pattern analyses and genetic interpretation about the geotectonics of Yudong (East Chongqing). Geotectonica Et Metallogenia. 2004;**28**:15-22

[30] Guo JH, Zhu MH, Liu CS, Liu XF, Zhang HD, Wang MY. Structural characteristics of the corridor section in Sangzhi-Shimen synclinore. Geotectonica Et Metallogenia. 2005;**29**:215-222

[31] Yan DP, Wang XW, Liu YY. Analysis of fold style and its formation mechanism in the area of boundary among Sichuan, Hubei and Hunan. Geoscience. 2000;**14**:37-43

[32] Liu SG, Deng B, Zhong Y. Unique geological features of burial and superimposition of the lower Paleozoic shale gas across the Sichuan Basin and its periphery. Earth Science Frontiers. 2016;**23**:11-28

[33] Guo TL, Zeng P. The structural and preservation conditions for shale gas enrichment and high productivith in the Wufeng-Longmaxi formation, southeastern Sichuan Basin. Energy Exploration and Exploitation. 2015;**33**:259-276

[34] Ma Y, Zhong NN, Han H. Definition and sturcture characteristics of pores in mylonitized organic-rich shales. Science China: Earth Sciences. 2014;**44**:2202-2209

[35] Wang ZX, Zhang J, Guan HM. A discussion on the structural deformation and oil/gas traps on the western side of the Xuefeng Mountain. Geological Bulletin of China. 2012;**31**:1812-1825

[36] Guo TL. Discovery and characteristics of the Fuling shale gas field and its enlightenment and thinking. Earth Science Frontiers. 2016;**23**:29-43

[37] Ibanez WD, Kronenberg AK. Experimental deformation of shale: Mechanical properties and micromechanical indicators of mechanisms. International Journal of Rock Mechanics and Mining Sciences & Geomechanics. 1993;**30**:723-734

[38] Ross DJK, Bustin RM. The importance of shale composition and pore structure upon gas storage potential of shale gas reservoirs. Marine and Petroleum Geology. 2009;**26**:916-927

[39] Pan JN, Hou QL, YW J, et al. Coalbed methane sorption related to coal deformation structures at different temperatures and pressures. Fuel. 2012;**102**:760-765

[40] Pan JN, Zhu HT, Hou QL. Macromolecular and pore structures of Chinese tectonically deformed coal studied by atomic force microscopy. Fuel. 2015;**139**:94-101

[41] Yan DP, Jin ZL, Zhang WC, Liu SF. Rock mechanical characteristics of the multi-layer detachment fault system and their controls on the structural deformation style of the Sichuan-Chongqing-Hunan-Hubei thin-skinned belt, South China. Geological Bulletin of China. 2008;**27**:1687-1697

[42] Feng XY, Meng XG, Shao ZG, Wang JP, Zhu DG. A preliminary discussion on features and dynamics of sequence deformation in South China and neighboring areas. Acta Geosicientia Sinica. 2003;**24**:115-120

[43] Wang YJ, Zhang YH, Fan WM, Peng TP. Structural signatures and 40Ar/ 39 Ar geochronology of the Indosinian Xuefengshan tectonic belt, South China block. Journal of Structural Geology. 2005;**27**:985-998

[44] Cai XL, Cao JM. The deformation structures framework control function on earthquake in Sichuan Basin. Earthquake Research in Sichuan. 1998;**3**:26-34

[45] Hu GC, Xie YX. The Steep Structures in the Carboniferous Gas Fields, Eastern Sichuan, China. Beijing: Petroleum Industry Press; 1997

[46] Wang YS, Wang XB, Gou L, Jia JD. Several progress of deep-shallow structure interpretation by MT along Songpan-Shaoyang cross section. South-to-north water transfers and. Water Science and Technology. 2007;**5**:70-77

[47] Washburn EW. The dynamics of capillary flow. Physics Review. 1921;**17**:273-283

[48] Clarkson CR, Haghshenas B, Ghanizadeh A. Nanopores to megafractures: Current challenges and methods for shale gas reservoir and hydraulic fracture characterization. Journal of Natural Gas Science and Engineering. 2016;**31**:612-657

[49] Thommes M, Kaneko K, Neimark AV. Physisorption of gases, with special reference to the evaluation of surface area and pore size distribution (IUPAC technical report). Pure and Applied Chemistry. 2015;**87**:1051-1069

[50] Chalmers GRL, Bustin RM, Bustin AAM. Geological controls on matrix permeability of the Doig-Montney hybrid shale-gas–tight-gas reservoir, northeastern British Columbia (NTS 093P). In: Geoscience BC Summary of Activities. Geoscience BC, Report 2012-1, 2011. pp. 87-96

[51] Liang ML, Wang ZX, Gao L. Evolution of pore structure in gas shale related to structural deformation. Fuel. 2017;**197**:310-319

[52] Jiang FJ, Chen D, Wang ZF. Pore characteristic analysis of a lacustrine shale: A case study in the Ordos Basin, NW China. Marine and Petroleum Geology. 2016;**73**:554-571

[53] Chen J, Xiao X. Evolution of nanoporosity in organic-rich shales during thermal maturation. Fuel. 2014;**129**:173-181

[54] Curtis ME, Cardott BJ, Sondergeld CH. Development of organic porosity in the Woodford shale with increasing thermal maturity. International Journal of Coal Geology. 2012;**103**:26-31

[55] Sun LN, Tuo JC, Zhang MF. Formation and development of the pore structure in Chang 7 member oil-shale from Ordos Basin during organic matter evolution induced by hydrous pyrolysis. Fuel. 2015;**158**:549-557

[56] Kareem R, Cubillas P, Gluyas J. Multi-technique approach to the Petrophysical characterization of Berea sandstone Core plugs (Cleveland quarries, USA). Journal of Petroleum Science and Engineering. 2017;**149**:436-455

[57] Luo QY, Zhong NN, Dai N. Graptolite-derived organic matter in the Wufeng–Longmaxi formations (upper Ordovician–lower Silurian) of southeastern Chongqing, China: Implications for gas shale evaluation. International Journal of Coal Geology. 2016;**153**:87-98

IntechOpen